ELSEVIER

Physica D 97 (1996) 509–516

PHYSICA D

Spirals in excitable media: the free-boundary limit with diffusion

David A. Kessler [a,*], Raz Kupferman [b]

[a] *Department of Physics, Bar-Ilan University, Ramat-Gan 52900, Israel*

[b] *AT&T Bell Laboratories, 600 Mountain Avenue, Murray Hill, New Jersey 07974, USA*

Received 18 September 1995; revised 4 December 1995; accepted 5 December 1995

Communicated by L. Kramer

Abstract

We solve numerically for the steady-state spiral in the thin-interface limit, including the effects of diffusion of the slow field. The calculation is performed using a generalization of the hybrid scheme of Keener. In this method, the diffusion equation is solved on a suitable mapped lattice while the eikonal equation relating the field on the interface to the interfacial velocity and curvature is solved independently. We present results for the selected frequency and tip radius as a function of the various parameters. We note that a stability analysis based on these results may be performed.

The study of spiral patterns in excitable media has been the focus of considerable attention in recent years (for a review, see [1]). Much progress has been achieved in this area, through the use of simulations and the analysis of various limiting cases. Spirals exhibit a wide range of interesting dynamics, including transitions from simple rotation to meandering (compound rotation) to hypermeandering and yet more complex behaviors [2,3]. Spirals are relevant not only in the context of chemical reactions such as the famed Belousov–Zhabotinskii reaction [2,4] but also in various biological systems such as electrical conduction in heart tissue [5] and aggregation of the slime mold [6].

A key tool for analyzing spirals, and patterns in general, is the thin-interface, or free-boundary limit. This limit arises [7] from taking the ratio, $1/\epsilon$, of the reaction rate of the bi-stable reaction to the other reaction to be large. In this limit, the dynamics reduces to that of the single "slow" field. The spiral can then be considered as a sharp interface between two different phases of the slow field, the so-called "excited" and "refractory" regions. In particular, there is much evidence to support the notion that in this limit, the spiral solution achieves a simple scaling form, known as the Fife ansatz [8], in which the parameter ϵ only determines the overall length and time scales of the pattern. In this limit, the spiral is characterized by only a few simple macroscopic "material parameters" derivable from the underlying dynamics.

This Fife-scaling has been verified in two limits. One is the limit where the diffusion constant of the slow field is vanishingly small [9–11]. In this limit, the "tip radius," the distance of closest approach of the spiral to the center of rotation, goes to zero. Also, the curvature at the tip goes to infinity. One then has to treat the tip region separately, with a cutoff length scale given by the larger of the small diffusion length or the small interface width. When one analyzes the stability of the spiral in this limit [12], one finds that the tip always exhibits a single unstable mode. It is

* Corresponding author.

PII S0167-2789(96)00135-2

difficult to square this behavior with that observed in simulations [13], where the spiral undergoes a Hopf bifurcation from steady rotation to meandering, which arises as a result of a complex conjugate *pair* of unstable modes. One is left to wonder whether this difference in dynamical behavior is a result of the Fife (small ϵ) limit or the small diffusion limit.

More recently, the Fife limit has been solved in a second limit, where the dynamics in the two phases is symmetrical [14]. In this limiting case, the tip radius and the curvature at the tip are both zero. While the dynamical stability of this solution has not been investigated, it appears from simulation that there is no meandering transition in this case [15]. This is in fact quite reasonable, since by symmetry the spiral cannot depart from the center of rotation. Thus, again, we are stymied in our attempt to understand the generic dynamics of the Fife regime and in particular the fate of the meandering transition in this limit. In order to achieve this aim, a necessary first step is to generate a solution of the steady-state spiral for finite diffusion and asymmetric dynamics. In the following we report on such a solution.

Let us first formulate the problem, so as to fix notation and terminology. We start from the two-variable reaction–diffusion system studied by Barkley [13]:

$$\dot{u} = \nabla^2 u + u(1-u)(u-(v+b)/a)/\epsilon, \tag{1a}$$

$$\dot{v} = D\nabla^2 v + u - v. \tag{1b}$$

The fast variable, u, by virtue of the smallness of ϵ, is always either 0 (refractory, "−") or 1 (excited, "+"), except for sharp transition regions of width $\sqrt{\epsilon}$. Thus, the u-field can be eliminated, resulting in the v-field dynamics,

$$\dot{v}_+ = D\nabla^2 v_+ + 1 - v_+, \tag{2a}$$

$$\dot{v}_- = D\nabla^2 v_- - v_-, \tag{2b}$$

in the two phases, respectively. The v-field is continuous and has continuous first derivative across the transition regions, or interfaces. The dynamics of these interfaces is given by the eikonal equation

$$c_n = -\kappa + v(v_{int})/\sqrt{\epsilon}, \tag{3}$$

whereby the normal velocity c_n of a given point on the interface is given by the interfacial curvature κ and the value of v at this point. We adopt the sign convention that the interface has positive velocity if the excited phase propagates into the refractory phase. Similarly, the interface curvature is positive when the excited region is convex. The function v can be computed from a study of soliton propagation in Eq. (1a). For our purposes, it is sufficient to replace v by its linear expansion around the stall value $v_s = \frac{1}{2}a - b$, where v vanishes, so that

$$v(v_{int}) = -\frac{\sqrt{2}}{a}(v_{int} - v_s). \tag{4}$$

As a can be eliminated by a rescaling we set $a = 1$. It is convenient at this point to shift the v-field by the constant v_s, yielding the equations

$$\dot{v}_\pm = D\nabla^2 v_\pm + g_\pm - v_\pm, \tag{5a}$$

$$c_n = -\kappa - \sqrt{2}\, v_{int}/\sqrt{\epsilon}, \tag{5b}$$

where $g_+ = 1 - v_s$, $g_- = -v_s$.

We are interested in steady-state spirals, rotating at constant frequency ω. The spiral consists of a "front," along which the excited phase invades the refractory phase, and a "back" along which the system reverts to the refractory state. The front and back meet at the spiral tip, where c_n vanishes, at a distance r_0 from the rotation center, which we may fix at the origin. Going into the corotating frame, with polar coordinates r and θ, our equations read

$$D\nabla^2 v_\pm + \omega\frac{dv_\pm}{d\theta} + g_\pm - v_\pm = 0, \tag{6a}$$

$$c_n = -\kappa - \frac{\sqrt{2}\, v_{int}}{\sqrt{\epsilon}}. \tag{6b}$$

This then is the system we shall study.

Fife [8] noticed that whereas ϵ appears explicitly in Eqs. (6), it can be eliminated through the rescaling of lengths by $\epsilon^{-1/6}$, time by $\epsilon^{-1/3}$ and the v-field by $\epsilon^{-1/3}$ so that $r \to \epsilon^{1/6} r$, $\omega \to \epsilon^{-1/3}\omega$, $c \to \epsilon^{-1/6} c$, $\kappa \to \epsilon^{-1/6}\kappa$, and $v \to \epsilon^{1/3} v$. Then, Eq. (6) reads

$$D\nabla^2 v_\pm + \omega\frac{dv_\pm}{d\theta} + g_\pm - \epsilon^{1/3} v_\pm = 0, \tag{7a}$$

$$c_n = -\kappa - \sqrt{2}\, v_{int}. \tag{7b}$$

Assuming that the rescaled v is O(1), we can drop the last term, in effect a "mass" term for the v-field, in Eq. (7a), yielding the ϵ-independent Fife equations

$$D\nabla^2 v_\pm + \omega \frac{\mathrm{d}v_\pm}{\mathrm{d}\theta} + g_\pm = 0\,, \tag{8a}$$

$$c_\mathrm{n} = -\kappa - \sqrt{2}\, v_\mathrm{int}\,. \tag{8b}$$

Note also, that the Fife-limit justifies our linearization of the function v in Eq. (4).

We now turn to a discussion of our numerical procedure for solving Eqs. (6) (and likewise (8)). The procedure is an extension of the one developed by Keener [14] in his study of Eqs. (6) in the symmetric limit $g_+ = -g_-$. The essential insight of Keener is that the diffusion equation (6a) is very difficult to treat due to the discontinuity of the operator along the as yet unknown interfaces. Furthermore, the eikonal equation (6b) refers to values of v along the interface, which will not necessarily pass through the grid points, so that a complicated interpolation scheme is required. Keener managed to eliminate both these obstacles in one fell swoop by mapping the plane as in Fig. 1(b), so that the excited (refractory) region is the lower (upper) half-plane. The spiral front and back are just the positive and negative x-axes in this new coordinate system. Keener noticed that if one knew the position of the spiral front, parameterized by $\theta_\mathrm{f}(r)$ (for a symmetric spiral, the back is given by $\theta_\mathrm{b} = \theta_\mathrm{f} + \pi$) then the polar coordinates (r, α), where

$$\alpha \equiv \theta - \theta_\mathrm{f}(r), \tag{9}$$

have just the required properties. The front maps to the line $\alpha = 0$, i.e. the positive x-axis and the back to $\alpha = \pi$, the negative x-axis. Also, so long as $\theta_\mathrm{f}(r)$ is monotonic, the mapping is 1–1 and onto. The calculation proceeds in an iterative fashion. Given an initial guess for the curve $\theta_\mathrm{f}(r)$ and ω, one can solve the diffusion equation (6a) in the mapped coordinate system. In particular, the solution gives v along the interface. This is used as input to the eikonal equation (6b) which for a given $v_\mathrm{int}(r)$ is an ordinary differential equation for the front $\theta_\mathrm{f}(r)$. There is a unique ω for which the eikonal equation has a solution. This value of ω and the associated solution for the front are then fed back as inputs to the next round of the procedure. The result converges after a few rounds, yielding a consistent solution of both halves of Eqs. (6).

The key to extending this procedure to the general asymmetric case is to construct a suitable mapping. Basically we wish to again consider a covering of the plane generated by rotates about the tip of the spiral front. To do this, we first pick a polar coordinate system (ρ, φ) centered at the spiral tip (Fig. 1(a)), defining

$$\begin{aligned} \rho\cos\varphi &= r\cos\theta - r_0, \\ \rho\sin\varphi &= r\sin\theta. \end{aligned} \tag{10}$$

In this coordinate system, the front and back are given by $\varphi_\mathrm{f}(\rho)$ and $\varphi_\mathrm{b}(\rho)$, with

$$\varphi_\mathrm{f}(0) = \tfrac{1}{2}\pi, \qquad \varphi_\mathrm{b}(0) = \tfrac{3}{2}\pi. \tag{11}$$

The remaining obstacle is that the front and back are no longer rotates of each other; i.e. $\varphi_\mathrm{b}(\rho) \neq \varphi_\mathrm{f}(\rho) + \pi$. Thus, if we were to adopt the Keener definition of α, Eq. (9), the front would again map to the ray $\alpha = 0$ (the positive x-axis), but the back would not map to the negative x-axis. To fix this, $\varphi(\alpha)$ must smoothly interpolate from $\varphi_\mathrm{f}(\rho)$ at $\alpha = 0$ to $\varphi_\mathrm{b}(\rho)$ at $\alpha = \pi$. A simple choice which satisfies this constraint is to define α implicitly by

$$\begin{aligned} \varphi \equiv{}& \alpha + \varphi_\mathrm{f}(\rho) \\ &+ (\varphi_\mathrm{b}(\rho) - \varphi_\mathrm{f}(\rho) - \pi)\sin^2\tfrac{1}{2}\alpha. \end{aligned} \tag{12}$$

The polar coordinates (ρ, α) thus map the asymmetric spiral to the x-axis as depicted in Fig. 1(b). It is easy to verify that α is a monotonic function of φ, so that the mapping is 1–1 and onto, so long as $|\varphi_\mathrm{b}(\rho) - \varphi_\mathrm{f}(\rho) - \pi|$ is everywhere less than 2. For very large asymmetry, this condition is violated, and a different mapping needs to be found for these cases. In any event, we will restrict our attention in this paper to moderate values of the asymmetry.

With the mapping in hand, we can proceed to the calculation. Instead of the iterative scheme employed by Keener, we have chosen to use a Newton's method approach. Given two trial interface curves $\varphi_\mathrm{f}(\rho)$ and $\varphi_\mathrm{b}(\rho)$ along with values for ω and r_0, we can calculate the field along the interface, $v_\mathrm{int}(\rho)$ in two independent ways. The first is from the diffusion equation (6a),

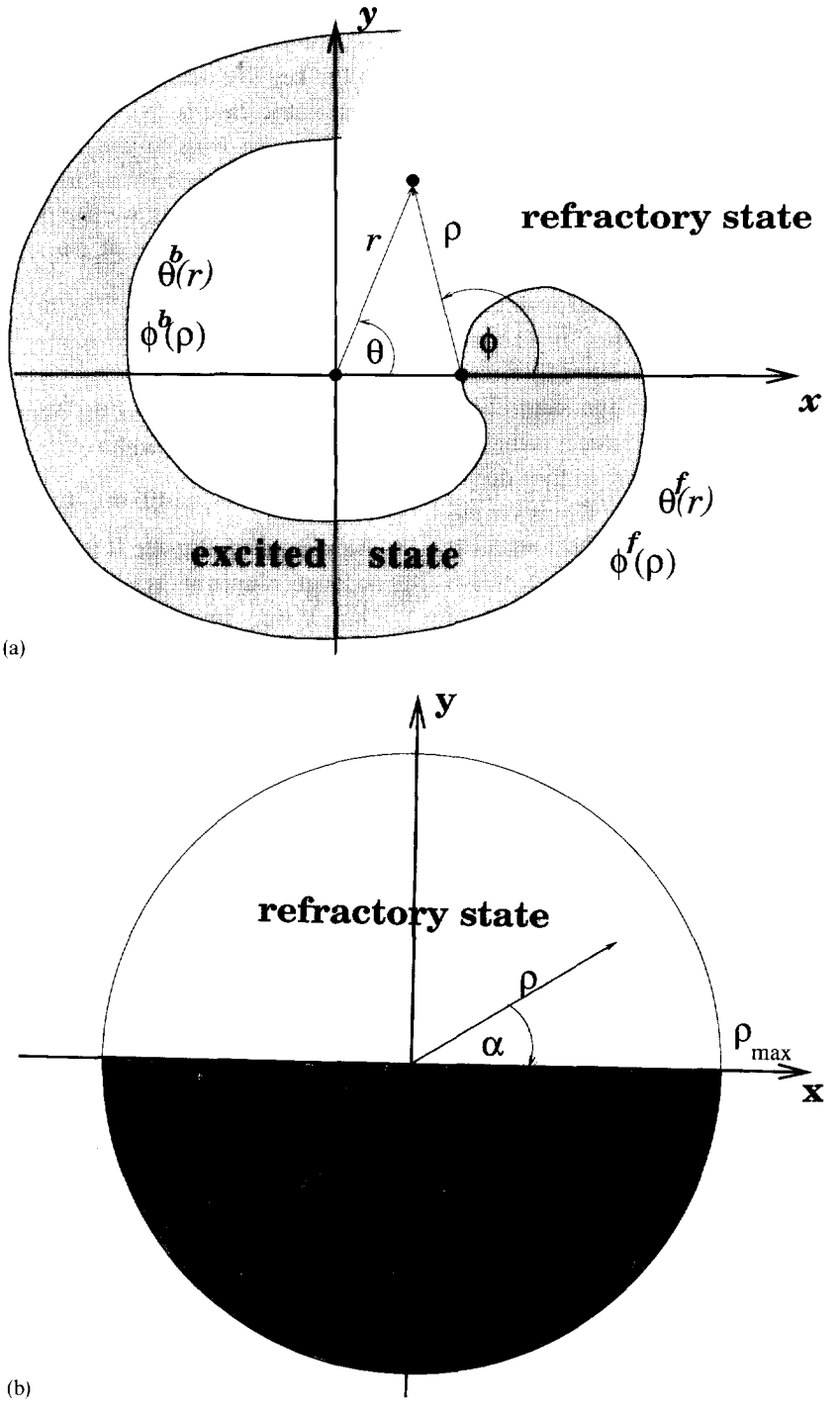

Fig. 1. (a) Schematic plot of the spiral geometry. (b) The mapping from the physical plane to the (ρ,α) plane.

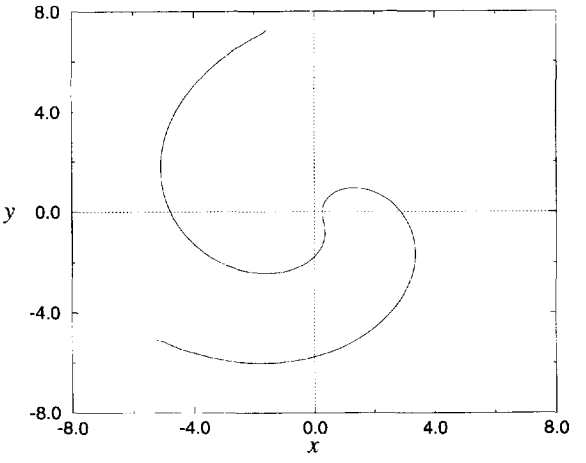

Fig. 2. The steady-state spiral for the parameters: $\epsilon = 0.02$, $D = 0.2$, $v_s = 0.4$.

transformed to the variables (ρ, α). (We present the transformed diffusion operator and some technical remarks, including a discussion of boundary conditions, in Appendix A.) The second method of calculating v_{int} is from the eikonal equation (6b), since v_{int} is determined from the interface curve via κ and c_n. In general, of course, the two determinations of v_{int} will yield differing results. In order to have a consistent solution, we have to find values of $\varphi_f(\rho)$, $\varphi_b(\rho)$, ω and r_0 such that the two calculations of v_{int} agree for all ρ. Thus, if we have a mesh of $N + 1$ points in ρ, we have $2N$ nonlinear equations ($2N - 2$ matching equations for v_{int} in the interior, one at the tip, and the smoothness condition $\varphi_f'(0) = -\varphi_b'(0)$) for the $2N$ variables ($N - 1$ interior values for each of φ_f and φ_b, ω and r_0). These equations are then solved via a Newton's method solver, starting from some initial guess.

We present in Fig. 2 the result of our calculation for the steady-state spiral shape for a typical set of parameters. We present in Fig. 3(a) a graph of ω vs. the asymmetry, $g_+ + g_-$, and in Fig. 3(b) the results for r_0 vs. the asymmetry. We see in agreement with expectation that the tip radius r_0 increases with increasing asymmetry. Also ω decreases with asymmetry, in accord with the result for the small diffusion limit of Keener [16], Karma [10] and Bernoff [9].

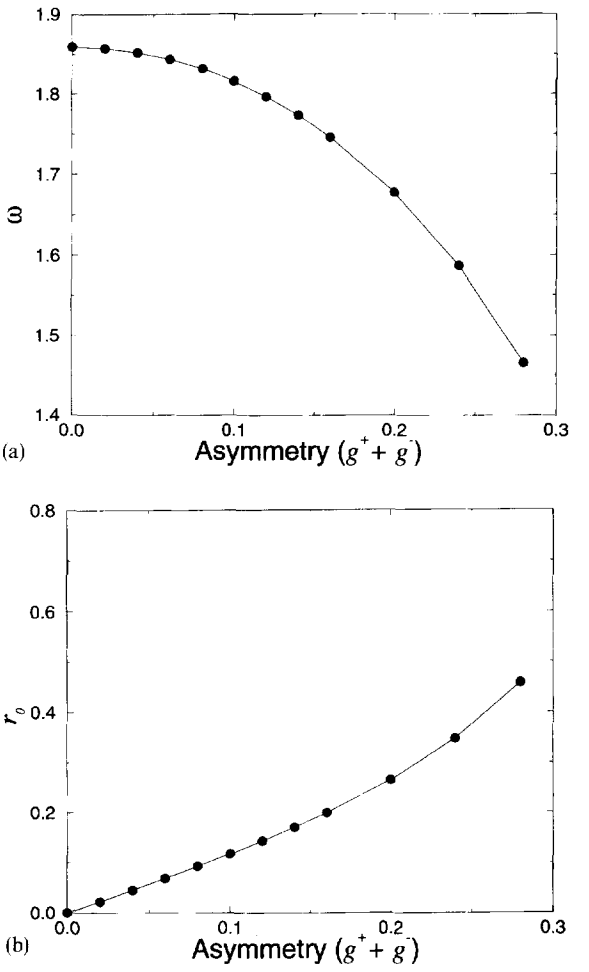

Fig. 3. (a) The spiral rotation frequency ω vs. asymmetry. (b) The tip radius r_0 vs. asymmetry, $g_+ + g_-$. Here, $\epsilon = 0.02$, $D = 0.2$.

In Fig. 4 we investigate the ϵ dependence of ω and r_0. We compare the results of solving Eq. (6) with those of the Fife-scaled equation (8). Here the answers are quite good for ϵ's less than about 1/100. We also present on this graph the results from a direct simulation of the original two-field model, Eq. (1), using Barkley's EZSPIRAL program. The results for the frequency ω are excellent, whereas those for r_0, while qualitatively correct, are off by about 50%. The reasons for this fairly large discrepancy needs to be better understood, though it is clear from the comparison to the Fife scaling that the tip radius is much more

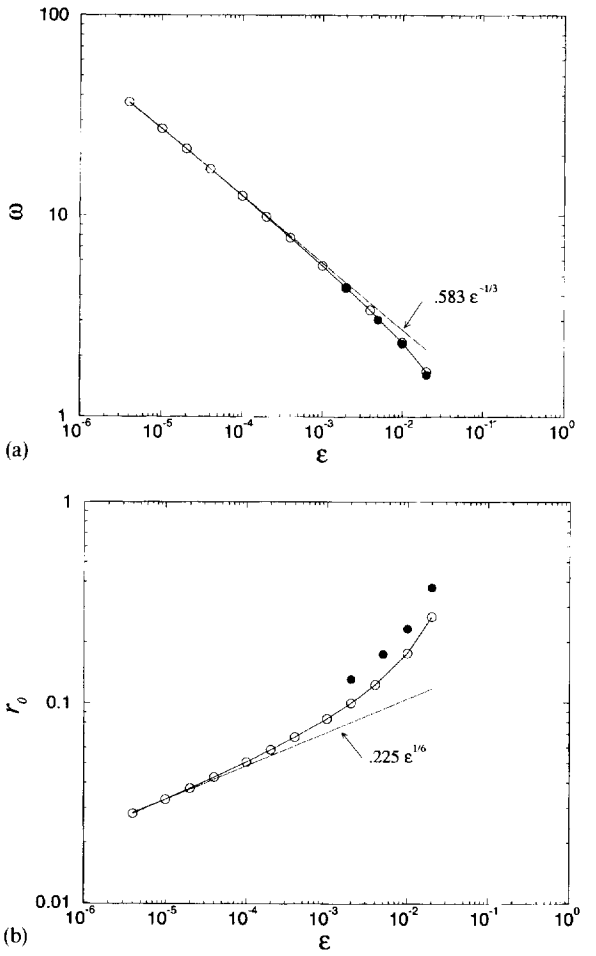

Fig. 4. (a) The spiral rotation frequency ω vs. ϵ. (b) The tip radius r_0 vs. ϵ. The numerical results are given by the open circles (connected by lines to guide the eye). The Fife scaling laws are shown by solid lines. The results of simulations are indicated by filled circles. Here, $D = 0.2$, $v_s = 0.4$.

sensitive to finite ϵ effects. The discrepancy conceivably could arise due to the linearization of the function v in the eikonal equation (6b).

The behavior of the solution with D is more interesting. We show in Fig. 5 a graph of r_0 (in Fife units, i.e. scaled by $\epsilon^{-1/6}$) vs. D for several values of ϵ, together with the prediction of Bernoff. We see that for any finite ϵ, r_0 approaches a constant as D goes to 0. This constant decreases with decreasing ϵ, vanishing (even in Fife units) only as ϵ goes to 0. (It is interesting to note that our numerical procedure has great difficulties when ϵ is smaller than about 10^{-20} (the source

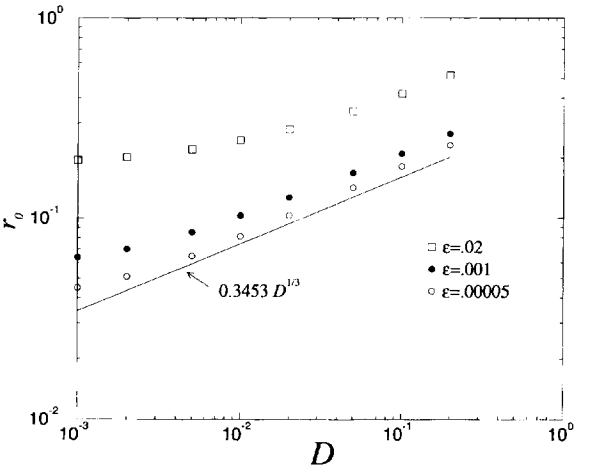

Fig. 5. The Fife-scaled tip radius $r_0(\text{Fife}) = r_0\epsilon^{-1/6}$ vs. D for $\epsilon = \{0.02, 0.001, 0.0005\}$. Here $v_s = 0.4$ The straight line is the prediction of the Bernoff theory.

of this problem and its implications are not yet clear). Thus the system adopts the Keener/Karma/Bernoff diffusionless outer solution only for zero ϵ (or, equivalently, zero "mass" term in Eq. (7a)). This is consistent with the observation that the Bernoff solution of the core region is only consistent for zero ϵ. If there were to be a mass term, then the leading order equation for v in the "core" region, $r < r_0$, is (in Fife units)

$$\omega \frac{\mathrm{d}v}{\mathrm{d}\theta} = v\epsilon^{1/3}, \tag{13}$$

which has no periodic solution. Thus, only if $\epsilon \lesssim O(D)$ is a Bernoff type core possible. For general ϵ, the system chooses to keep r_0 finite, with $\nabla^2 v$ going to infinity as D goes to 0. Of course, for sufficiently small D, finite interface width effects become critical and our reduction to a free boundary problem is rendered invalid. All this only serves to underscore how delicate the Bernoff limit is, with its requirement that $\epsilon^{1/3} \ll D^{1/3} \ll 1$. It is perhaps no surprise, then that the stability properties of the Bernoff solution are very atypical. It also raises the hope that a new kind of "diffusionless" core, in the presence of a finite mass term, might be found, whose properties would more closely correspond to those of the generic spiral.

While these results are instructive, their true importance lies in the fact that they are an essential prerequisite for the study of the many open questions regarding

spiral stability and dynamics. A linear stability analysis may be constructed using the same hybrid formulation we have used for the steady-state calculation. Work along these lines is proceeding apace.

Acknowledgements

DAK acknowledges useful conversations with J. Schiff and H. Levine. He also acknowledges the support of the Raschi Foundation. DAK and RK acknowledge the support of Grant No. 9200051 from the United States – Israel Binational Science Foundation (BSF).

Appendix A

We may express the diffusion equation (6a) in the transformed variables (ρ,α) as

$$D\left[\frac{\partial^2 v}{\partial\rho^2}+\frac{1}{\rho}\frac{\partial v}{\partial\rho}+f_1(\rho,\alpha)\frac{\partial^2 v}{\partial\alpha^2}+f_2(\rho,\alpha)\frac{\partial v}{\partial\alpha}+f_3(\rho,\alpha)\frac{\partial^2 v}{\partial\rho\partial\alpha}\right]+\omega\left[f_4(\rho,\alpha)\frac{\partial v}{\partial\rho}+f_5(\rho,\alpha)\frac{\partial v}{\partial\alpha}\right]+g_{\pm}-v=0. \tag{A.1}$$

The coefficient functions f_i can be most conveniently expressed in terms of the following derivatives of the mapping $\alpha(\rho,\varphi)$:

$$g_1\equiv\left(\frac{\partial\alpha}{\partial\rho}\right)_{\varphi}=-\frac{\varphi_{\mathrm{f}}'(\rho)+[\varphi_{\mathrm{b}}'(\rho)-\varphi_{\mathrm{f}}'(\rho)]\sin^2\frac{1}{2}\alpha}{1+\frac{1}{2}[\varphi_{\mathrm{b}}(\rho)-\varphi_{\mathrm{f}}(\rho)-\pi]\sin\alpha},$$

$$g_2\equiv\left(\frac{\partial\alpha}{\partial\varphi}\right)_{\rho}=\frac{1}{1+\frac{1}{2}[\varphi_{\mathrm{b}}(\rho)-\varphi_{\mathrm{f}}(\rho)-\pi]\sin\alpha},$$

$$g_3\equiv\left(\frac{\partial g_2}{\partial\alpha}\right)_{\rho}=-\frac{\frac{1}{2}[\varphi_{\mathrm{b}}(\rho)-\varphi_{\mathrm{f}}(\rho)-\pi]\cos\alpha}{\left\{1+\frac{1}{2}[\varphi_{\mathrm{b}}(\rho)-\varphi_{\mathrm{f}}(\rho)-\pi]\sin\alpha\right\}^2},$$

$$g_4\equiv\left(\frac{\partial g_1}{\partial\rho}\right)_{\alpha}=-g_2\left\{\left[\varphi_{\mathrm{f}}''+(\varphi_{\mathrm{b}}''-\varphi_{\mathrm{f}}'')\sin^2\tfrac{1}{2}\alpha\right]+\tfrac{1}{2}g_1(\varphi_{\mathrm{b}}'-\varphi_{\mathrm{f}}')\sin\alpha\right\},$$

$$g_5\equiv\left(\frac{\partial g_1}{\partial\alpha}\right)_{\rho}=-\tfrac{1}{2}g_2\left\{(\varphi_{\mathrm{b}}'-\varphi_{\mathrm{f}}')\sin\alpha+g_1(\varphi_{\mathrm{b}}-\varphi_{\mathrm{f}}-\pi)\cos\alpha\right\}. \tag{A.2}$$

Then

$$\begin{aligned}f_1&=g_1^2+g_2^2/\rho^2,\\ f_2&=g_4+g_1g_5+g_1/\rho+g_2g_3/\rho^2,\\ f_3&=2g_1,\\ f_4&=r_0\sin\varphi,\\ f_5&=r_0\sin\varphi\,g_1+(1+(r_0/\rho)\cos\varphi)g_2.\end{aligned} \tag{A.3}$$

Similarly, the normal velocity, c_{n}, is given in the mapped coordinates by

$$c_{\mathrm{n}}=\pm\omega\frac{\rho+r_0\cos\varphi_{\mathrm{f,b}}-\rho r_0\varphi_{\mathrm{f,b}}'\sin\varphi_{\mathrm{f,b}}}{[1+(\rho\varphi_{\mathrm{f,b}}')^2]^{1/2}}, \tag{A.4}$$

and the curvature, κ by

$$\kappa=\pm\frac{-\rho^2(\varphi_{\mathrm{f,b}}')^3-\rho\varphi_{\mathrm{f,b}}''-2\varphi_{\mathrm{f,b}}'}{[1+(\rho\varphi_{\mathrm{f,b}}')^2]^{3/2}}, \tag{A.5}$$

where the "+" ("−") refers to the front (back) respectively.

We need to specify boundary conditions for our solution of both the diffusion (A.1) and eikonal (6b) equations. We solve the diffusion equation on the interval $\rho\in(0,\rho_{\max})$ where we choose $\rho_{\max}$ sufficiently large so that the spiral completes one turn. We use no-flux boundary conditions on the outer boundary, requiring $\partial v/\partial\rho$ to vanish at $\rho_{\max}$. Note that the boundary is circular in the coordinates (ρ,α), so that

it is deformed (and co-rotating with the spiral) in the original frame of reference. Nevertheless, as we expect the dependence on the outer boundary to be exponentially suppressed, we do not expect the exact nature of the boundary conditions to be relevant. Indeed we verify that increasing $\rho_{\max}$ has a negligible effect on the selected ω. We require v to be regular at the origin. We accomplish this by rewriting Eq. (A.1) at $\rho = 0$ using Green's theorem to re-express the Laplacian as

$$\nabla^2 v_{\rho=0} \approx \frac{2}{\pi \Delta\rho} \left\{ \int_0^{2\pi} \left(\frac{\partial\varphi}{\partial\alpha}\right)_\rho \mathrm{d}\alpha \times \left[\left(\frac{\partial v}{\partial\rho}\right)_\alpha + \left(\frac{\partial\alpha}{\partial\rho}\right)_\varphi \left(\frac{\partial v}{\partial\alpha}\right)_\rho \right] \right\}_{\rho=\Delta\rho/2}, \tag{A.6}$$

where $\Delta\rho$ is the lattice spacing in ρ.

For the eikonal equation, we require φ_{f}' and φ_{b}' to vanish at the outer boundary. We require the curve to be twice differentiable everywhere in its interior, including at the tip. This condition, as noted in the text, provides one of the equations needed in our method. We also point out that our geometry fixes the requirement that $\varphi_{\mathrm{f}}(0) = \frac{1}{2}\pi$, and $\varphi_{\mathrm{b}}(0) = \frac{3}{2}\pi$.

The results presented in this paper were obtained using 50 lattice points in α and 50 in ρ. We found these sufficient to generate answers correct to the 1% level.

References

[1] E. Meron, Phys. Rep. 218 (1992) 1.
[2] G.S. Skinner and H.L. Swinney, Physica D 48 (1990) 1.
[3] A. Winfree, Chaos 1 (1991) 303.
[4] T. Plesser, S.C. Müller and B. Hess, J. Phys. Chem. 94 (1990) 7501; J. Ross, S.C. Müller and C. Vidal, Science 240 (1988) 460.
[5] A.M. Pertsov et. al., Circulation Research 72 (1993) 631; I.R. Efimov, V.I. Krinsky and J. Jalife, Chaos, Solitons and Fractals 5 (1995) 513; A. Karma, Phys. Rev. Lett. 71 (1993) 1103.
[6] J.-L. Martiel and A. Goldbeter, Biophys. J. 52 (1987) 807; J.J. Tyson, K.A. Alexander, V.S. Manoranjan and J.D. Murray, Physica D 34 (1989) 193.
[7] J.P. Keener, SIAM J. Appl. Math. 46 (1986) 1039.
[8] P.C. Fife, in: Non-Equilibrium Dynamics in Chemical Systems eds. C. Vidal and A. Pacault (Springer, New York, 1984).
[9] A.J. Bernoff, Physica D 53 (1991) 125.
[10] A. Karma, Phys. Rev. Lett. 68 (1992) 401.
[11] D.A. Kessler, H. Levine and W.N. Reynolds, Phys. Rev. Lett. 68 (1992) 401.
[12] D.A. Kessler, H. Levine and W.N. Reynolds, Phys. Rev. A 46 (1992) 5264; D.A. Kessler, H. Levine and W.N. Reynolds, Physica D 70 (1994) 115.
[13] D. Barkley, Phys. Rev. Lett. 68 (1992) 2090.
[14] J.P. Keener, Physica D 70 (1994) 61.
[15] D.A. Kessler, unpublished.
[16] J.J. Tyson and J.P. Keener, Physica D 32 (1988) 327.